

## PAPER

# Modeling and Analysis of Electromechanical Automatic Leveling Mechanism for High-Mobility Vehicle-Mounted Theodolites

Xiangyu LI<sup>†,††,†††a)</sup>, Ping RUAN<sup>†,††b)</sup>, Wei HAO<sup>†,††c)</sup>, Meilin XIE<sup>†,††d)</sup>, and Tao LV<sup>†,††,†††e)</sup>, *Nonmembers*

**SUMMARY** To achieve precise measurement without landing, the high-mobility vehicle-mounted theodolite needs to be leveled quickly with high precision and ensure sufficient support stability before work. After the measurement, it is also necessary to ensure that the high-mobility vehicle-mounted theodolite can be quickly withdrawn. Therefore, this paper proposes a hierarchical automatic leveling strategy and establishes a two-stage electromechanical automatic leveling mechanism model. Using coarse leveling of the first-stage automatic leveling mechanism and fine leveling of the second-stage automatic leveling mechanism, the model realizes high-precision and fast leveling of the vehicle-mounted theodolites. Then, the leveling control method based on repeated positioning is proposed for the first-stage automatic leveling mechanism. To realize the rapid withdrawal for high-mobility vehicle-mounted theodolites, the method ensures the coincidence of spatial movement paths when the structural parts are unfolded and withdrawn. Next, the leg static balance equation is constructed in the leveling state, and the support force detection method is discussed in realizing the stable support for vehicle-mounted theodolites. Furthermore, a mathematical model for “false leg” detection is established furtherly, and a “false leg” detection scheme based on the support force detection method is analyzed to significantly improve the support stability of vehicle-mounted theodolites. Finally, an experimental platform is constructed to perform the performance test for automatic leveling mechanisms. The experimental results show that the leveling accuracy of established two-stage electromechanical automatic leveling mechanism can reach  $3.6''$ , and the leveling time is no more than 2 mins. The maximum support force error of the support force detection method is less than 15%, and the average support force error is less than 10%. In contrast, the maximum support force error of the drive motor torque detection method reaches 80.12%, and its leg support stability is much less than the support force detection method. The model and analysis method proposed in this paper can also be used for vehicle-mounted radar, vehicle-mounted laser measurement devices, vehicle-mounted artillery launchers and other types of vehicle-mounted equipment with high-precision and high-mobility working requirements.

**key words:** *vehicle-mounted theodolite, automatic leveling, support platform, static analysis, “false leg” detection*

## 1. Introduction

Vehicle-mounted theodolites are mainly used to record pa-

rameters such as the target trajectory, flight attitude, and radiation characteristics [1]. In recent years, besides the important development of the application field and observation capability [2], [3], the measurement method of vehicle-mounted theodolites has also undergone significant changes, gradually developing from the fixed ground type to the vehicle-mounted mobile type [4], [5]. The vehicle-mounted mobile type has the characteristics of rapid unfolding, rapid withdrawal, and no stagnation points, which has become the main use of vehicle-mounted theodolites at present [6], [7].

As an optical precision measurement equipment, the theodolite needs to be leveled with high precision before work so that its vertical axis coincides with the earth plumb line to ensure its measurement accuracy. Thus, when working without landing, the vehicle-mounted theodolite is generally roughly leveled with a hydraulic or electromechanical automatic leveling mechanism as the first-stage leveling mechanism [8]–[13], so that the tilt error of the vertical axis does not exceed  $3'$ . Then, the second-stage leveling mechanism of theodolites is used for precision leveling [14]–[17], so that the tilt error of the vertical axis is reduced to  $5''$ . However, affected by foundation settlement, wind load, operator activities and other factors, it is difficult for the first-stage leveling mechanism to achieve a high-precision leveling error of no more than  $5''$ . Meanwhile, the second-stage leveling mechanism is usually manual, and it takes 10 mins~20 mins for an experienced operator to adjust the leveling error to no more than  $5''$ . However, when the target is rapidly transferred to another location and rapidly launched, the high-mobility vehicle-mounted theodolite will be struggling to record parameters such as the target trajectory, flight attitude, and radiation characteristics due to the time-consuming problem of unfolding. It is obvious that that high-precision fast leveling is one of the important factors affecting the rapid unfolding performance and precision measurement capabilities of high-mobility vehicle-mounted theodolites.

Since the tilt of the vehicle support platform usually reaches several minutes or even a few degrees, the leveling of the theodolite support platform by the first-stage leveling mechanism often requires a wide range of translational and rotational movements for structural parts in space. Thus, how to ensure the spatial movement path coincidence of each structural part when unfolding and withdrawing is of great significance to the fast withdrawal performance emphasized for high-mobility vehicle-mounted theodolite.

The difference in support forces between the legs of the

Manuscript received May 22, 2023.

Manuscript revised August 21, 2023.

Manuscript published September 26, 2023.

<sup>†</sup>The authors are with Xi'an Institute of Optics and Precision Mechanics, Chinese Academy of Sciences, Xi'an, 710119, China.

<sup>††</sup>The authors are with Key Laboratory of Space Precision Measurement Technology, Xi'an Institute of Optics and Precision Mechanics, Chinese Academy of Sciences, Xi'an, 710119, China.

<sup>†††</sup>The authors are with University of Chinese Academy of Sciences, Beijing, 100049, China.

a) E-mail: lixiangyu@opt.ac.cn

b) E-mail: ruanp@opt.ac.cn (Corresponding author)

c) E-mail: haowei@opt.ac.cn

d) E-mail: xiemeilin6@163.com

e) E-mail: lvtao@opt.ac.cn

DOI: 10.1587/transfun.2023EAP1058

first-stage leveling mechanism will cause different shaking errors when the theodolite support platform is affected by disturbance factors such as wind load and its driving torque. The error amount generally varies from a few seconds to a few minutes. Especially, if there is a “false leg” in the first-stage mechanism, the support platform will be affected by disturbance factors that will cause instability or even overturning. At the same time, the shaking of the support platform will cause the theodolite to produce pitch and azimuth pointing angle errors. The results often do not meet the requirements of high-precision measurement, which requires the correction of angle measurement value for theodolites [18]–[25]. Therefore, the leg support force is one of the important factors affecting the high-precision measurement of vehicle-mounted theodolites.

This paper proposes a hierarchical automatic leveling strategy and establishes a two-stage electromechanical automatic leveling mechanism to achieve high-precision and fast leveling for vehicle-mounted theodolites by combining coarse leveling and fine leveling. The contribution in this paper is given as follows. (1) The leveling control method based on repeated positioning is proposed for the first-stage automatic leveling mechanism, which ensures the rapid withdrawal of theodolites by controlling the coincidence of spatial movement paths when the structural parts are unfolded and withdrawn. (2) The leg static balance equation and the mathematical model of “false leg” detection are established. Then, the “false leg” detection based on the support force detection method is analyzed to accurately control the landing support force of the legs. (3) A performance test of the automatic leveling mechanism is conducted to highlight the substantial effect achieved by the proposed leveling strategy and electromechanical automatic leveling mechanism. The test conducted in the paper is under outdoor environment, which would make the electromechanical automatic leveling mechanism more promising for engineering applications.

The rest of the paper is organized as follows. In Sect. 2, the non-landing measurement structure form of the vehicle-mounted theodolite is given. In Sect. 3, the first-stage automatic leveling mechanism design is presented. In Sect. 4, the second-stage automatic leveling mechanism design is presented. The “False leg” detection is shown in Sect. 5. A performance test of the automatic leveling mechanism is discussed in Sect. 6. At last, Sect. 7 gives the conclusion.

## 2. Non-Landing Measurement Structure Form of the Vehicle-Mounted Theodolite

The non-landing measurement structure form of the vehicle-mounted theodolite can be divided into two types: vehicle support type and theodolite support type according to the different support methods, as shown in Fig. 1.

The vehicle support type uses legs mounted on the vehicle frame to hold up vehicles. This form has a simple structure design, a large installation space and a flexible installation method for an automatic leveling mecha-

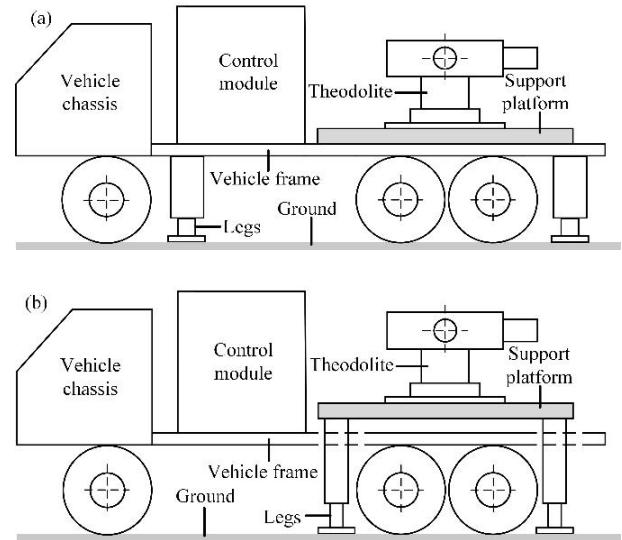


**Fig. 1** Non-landing measurement structure form of the vehicle-mounted theodolite. (a) Vehicle support type, (b) theodolite support type.

nism. However, because the legs support the whole vehicle, the complex structure composition and disturbance factors cause the first-stage leveling mechanism can only achieve 3' leveling accuracy. At the same time, due to the large cross-sectional area of vehicles, the theodolite is easily affected by wind loads during measurement. Moreover, the movement of operators on the vehicle and the deformation of the vehicle body caused by internal and external heat radiation all affect the measurement accuracy of the theodolite.

The theodolite support type uses the legs installed in the support platform to support the theodolite and detach it from the vehicle body, which can overcome the influence of shaking errors caused by the operators' movement. Because the load supported by legs is greatly reduced compared with the vehicle support type, the support legs can choose a economical smaller model. Moreover, the wobble error caused by wind loads, internal and external heat radiation is much smaller than that of the vehicle support type. The legs directly support the theodolite through the support platform, which reduces the complexity of non-landing measurement structure and can improve the adjustment accuracy of first-stage leveling. This paper chooses theodolite support type to start the modeling and analysis of the electromechanical automatic leveling mechanism.

## 3. First-Stage Automatic Leveling Mechanism Design

### 3.1 First-Stage Automatic Leveling Mechanism Model

As shown in Fig. 2, the physical model of the first-stage automatic leveling mechanism consists of a support platform, four electromechanical leveling legs, a tilt sensor and a leveling control module. The electromechanical leveling legs include drive motor, worm wheel, worm, force sensor, screw-nut pair and support ball hinge [26]–[28]. Vehicle-mounted theodolite does not fall to the ground for mea-

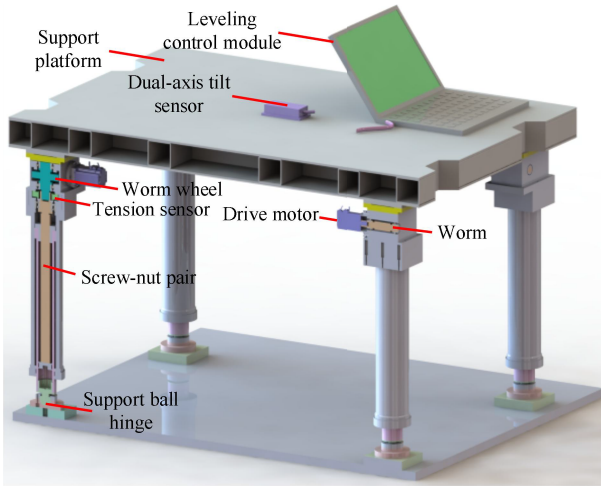


Fig. 2 Physical model of the first-stage automatic leveling mechanism.

surement, the four electromechanical leveling legs touch the ground to support the support platform. And the tilt sensor is used to transmit the horizontal tilt attitude information of the support platform to the leveling control module in real-time. The feedback signal from the tilt sensor drives the legs to achieve the first-stage rough leveling of vehicle-mounted theodolites.

As shown in Fig. 3, the physical model of the first-stage automatic leveling mechanism is geometrically simplified, and a Cartesian coordinate system is established with the horizontal plane and the earth plumb line as the reference. Specify the angle counterclockwise is positive. To facilitate the calculation of the spatial coordinates of the points in the geometric model in different states, assumed that the support surface of the vehicle is an absolute plane, so that the equivalent contact center points are in the same surface. Further, define the included angles between the support surface and the coordinate axis are  $\theta_x$  and  $\theta_y$  respectively.

Assuming that the equivalent contact center point O of leg 1 after touching the ground does not move during the leveling process of the first-stage automatic leveling mechanism. In the initial state, after the legs touch the ground to support the support platform, the legs  $OH_1$ ,  $U_1J_1$ ,  $V_1K_1$  and  $W_1Q_1$  are perpendicular to the support surface, and the support platform  $H_1J_1K_1Q_1$  is parallel to the support surface.

When the first-stage automatic leveling mechanism levels the support platform, by controlling the expansion and contraction of the legs, the legs and the support platform produce spatial translation and rotation, thereby realizing the leveling of the support platform. At this time, the legs  $OH_2$ ,  $U_2J_2$ ,  $V_2K_2$  and  $W_2Q_2$  after the change in spatial position are perpendicular to the horizontal plane, the support platform  $H_2J_2K_2Q_2$  is parallel to the horizontal plane, and the projection points of the legs  $U_2J_2$ ,  $V_2K_2$  and  $W_2Q_2$  on the horizontal plane are  $U_3$ ,  $V_3$  and  $W_3$ .

Assuming that the distance between the equivalent contact center points of the support platform and the legs are

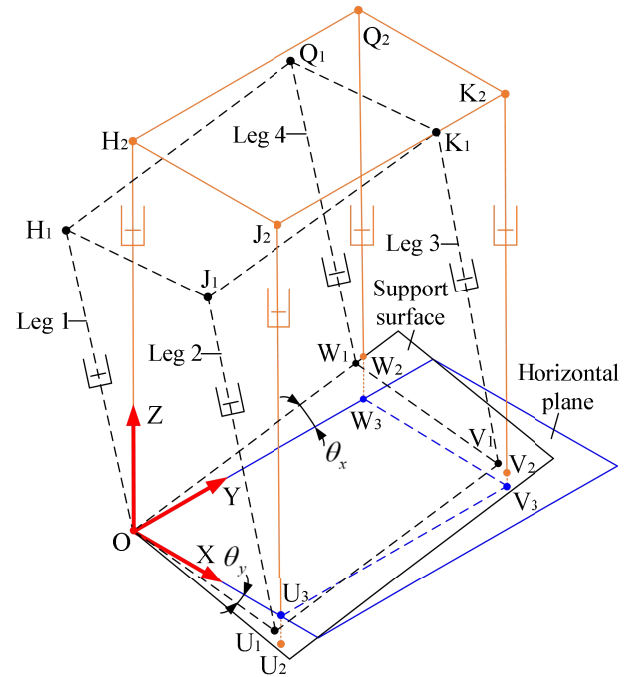


Fig. 3 Geometric model of the first-stage automatic leveling mechanism.

$$\begin{cases} H_1J_1 = Q_1K_1 = H_2J_2 = Q_2K_2 = L_1 \\ H_1Q_1 = J_1K_1 = H_2Q_2 = J_2K_2 = L_2 \end{cases} \quad (1)$$

When the support ball hinge support touches the ground, the distance between the equivalent contact center points is

$$\begin{cases} OU_1 = W_1V_1 = L_1 \\ OW_1 = U_1V_1 = L_2 \end{cases} \quad (2)$$

Compared to the earth's horizontal plane, assuming the plane  $OU_1V_1W_1$  is formed after first rotating  $\theta_x$  and then rotating  $\theta_y$ , corresponding to the rotation matrix is

$$R_x = \begin{bmatrix} 1 & 0 & 0 \\ 0 & \cos \theta_x & -\sin \theta_x \\ 0 & \sin \theta_x & \cos \theta_x \end{bmatrix} \quad (3)$$

$$R_y = \begin{bmatrix} \cos \theta_y & 0 & \sin \theta_y \\ 0 & 1 & 0 \\ -\sin \theta_y & 0 & \cos \theta_y \end{bmatrix} \quad (4)$$

The positional transformation matrix of any point on the plane  $OU_1V_1W_1$  is

$$R_{xy} = R_yR_x \quad (5)$$

When the support platform is leveled, the coordinates of  $H_2$ ,  $J_2$ ,  $K_2$  and  $Q_2$ , the coordinates of projection points O,  $U_2$ ,  $V_2$  and  $W_2$  for  $H_2$ ,  $J_2$ ,  $K_2$  and  $Q_2$  in the XOY plane can be obtained from Eqs. (6) and (7).

$$\begin{cases} (X_{H_2} \ Y_{H_2} \ Z_{H_2}) = (0 \ 0 \ H_{00}) \\ (X_{J_2} \ Y_{J_2} \ Z_{J_2}) = (L_1 \ 0 \ H_{00}) \\ (X_{K_2} \ Y_{K_2} \ Z_{K_2}) = (L_1 \ L_2 \ H_{00}) \\ (X_{Q_2} \ Y_{Q_2} \ Z_{Q_2}) = (0 \ L_2 \ H_{00}) \end{cases} \quad (6)$$

$$\begin{cases} \begin{pmatrix} X_O & Y_O & Z_O \end{pmatrix} = \begin{pmatrix} 0 & 0 & 0 \end{pmatrix} \\ \begin{pmatrix} X_{U_2} & Y_{U_2} & Z_{U_2} \end{pmatrix} = \begin{pmatrix} L_1 & 0 & 0 \end{pmatrix} \\ \begin{pmatrix} X_{V_2} & Y_{V_2} & Z_{V_2} \end{pmatrix} = \begin{pmatrix} L_1 & L_2 & 0 \end{pmatrix} \\ \begin{pmatrix} X_{W_2} & Y_{W_2} & Z_{W_2} \end{pmatrix} = \begin{pmatrix} 0 & L_2 & 0 \end{pmatrix} \end{cases} \quad (7)$$

The corresponding coordinates of  $U_1$ ,  $V_1$  and  $W_1$  are

$$\begin{bmatrix} X_{U_1} \\ Y_{U_1} \\ Z_{U_1} \end{bmatrix} = R_{xy} \begin{bmatrix} L_1 \\ 0 \\ 0 \end{bmatrix} \quad (8)$$

$$\begin{bmatrix} X_{V_1} \\ Y_{V_1} \\ Z_{V_1} \end{bmatrix} = R_{xy} \begin{bmatrix} L_1 \\ L_2 \\ 0 \end{bmatrix}. \quad (9)$$

$$\begin{bmatrix} X_{W_1} \\ Y_{W_1} \\ Z_{W_1} \end{bmatrix} = R_{xy} \begin{bmatrix} 0 \\ L_2 \\ 0 \end{bmatrix} \quad (10)$$

The equation of plane  $U_1V_1W_1$  is

$$\tan \theta_y \cdot X - \frac{\tan \theta_x}{\cos \theta_y} \cdot Y + Z = 0 \quad (11)$$

Coordinates of projection points  $U_3$ ,  $V_3$  and  $W_3$  for  $J_2$ ,  $K_2$  and  $Q_2$  on the support plane  $U_1V_1W_1$  are

$$\begin{bmatrix} X_{U_3} \\ Y_{U_3} \\ Z_{U_3} \end{bmatrix} = \begin{bmatrix} L_1 \\ 0 \\ -\tan \theta_y \cdot L_1 \end{bmatrix} \quad (12)$$

$$\begin{bmatrix} X_{V_3} \\ Y_{V_3} \\ Z_{V_3} \end{bmatrix} = \begin{bmatrix} L_1 \\ L_2 \\ \frac{\tan \theta_x \cdot L_2 - \sin \theta_y \cdot L_1}{\cos \theta_y} \end{bmatrix} \quad (13)$$

$$\begin{bmatrix} X_{W_3} \\ Y_{W_3} \\ Z_{W_3} \end{bmatrix} = \begin{bmatrix} 0 \\ L_2 \\ \frac{\tan \theta_x \cdot L_2}{\cos \theta_y} \end{bmatrix} \quad (14)$$

Assume that after the legs touch the ground and before the automatic leveling starts, the following relation holds.

$$OH_1 = H_0 \quad (15)$$

The corresponding coordinates of  $H_1$ ,  $J_1$ ,  $K_1$  and  $Q_1$  are

$$\begin{bmatrix} X_{H_1} \\ Y_{H_1} \\ Z_{H_1} \end{bmatrix} = R_{xy} \begin{bmatrix} 0 \\ 0 \\ H_0 \end{bmatrix} \quad (16)$$

$$\begin{bmatrix} X_{J_1} \\ Y_{J_1} \\ Z_{J_1} \end{bmatrix} = \begin{bmatrix} X_{U_1} \\ Y_{U_1} \\ Z_{U_1} \end{bmatrix} + \begin{bmatrix} X_{H_1} \\ Y_{H_1} \\ Z_{H_1} \end{bmatrix} \quad (17)$$

$$\begin{bmatrix} X_{K_1} \\ Y_{K_1} \\ Z_{K_1} \end{bmatrix} = \begin{bmatrix} X_{V_1} \\ Y_{V_1} \\ Z_{V_1} \end{bmatrix} + \begin{bmatrix} X_{H_1} \\ Y_{H_1} \\ Z_{H_1} \end{bmatrix} \quad (18)$$

$$\begin{bmatrix} X_{Q_1} \\ Y_{Q_1} \\ Z_{Q_1} \end{bmatrix} = \begin{bmatrix} X_{W_1} \\ Y_{W_1} \\ Z_{W_1} \end{bmatrix} + \begin{bmatrix} X_{H_1} \\ Y_{H_1} \\ Z_{H_1} \end{bmatrix} \quad (19)$$

Since the corresponding support ball hinge is not solidly connected to the support platform after the leg touches the ground. The equivalent contact center points of leg 2, leg 3 and leg 4 all move after landing during the leveling process. The equivalent contact center point of leg 2 moves from  $U_1$  to  $U_3$ , leg 3 moves from  $V_1$  to  $V_3$  and leg 4 moves from  $W_1$  to  $W_3$ . The corresponding leg movements can be obtained from the coordinate equations of  $U_1$ ,  $V_1$ ,  $W_1$ ,  $U_3$ ,  $V_3$  and  $W_3$ .

The geometric model of the first-stage automatic leveling mechanism can be used to obtain the spatial coordinates and position relationships of each equivalent contact center point in the initial and leveling states. However, this model is an open-analysis model. The leveling control strategy needs to be analyzed to model the leveling mechanism more accurately. In addition, the leveling control process is needed to optimize to ensure that the spatial movement path of each equivalent contact center point is controllable during the leveling process.

### 3.2 Leveling Control Method Based on Repeated Positioning

As shown in Fig. 4, ensuring that the locking mechanism between the support platform and the vehicle frame is accurately locked at the position of the release hook and the fixed hook is the core part of the rapid withdrawal for the vehicle-mounted theodolite. If the release hook and the fixed hook cannot be accurately aligned, the support platform and the vehicle frame cannot be fixed. Vehicle-mounted theodolite cannot be withdrawn quickly after completing the task. The calculation results of spatial coordinates and position relationship of each equivalent contact center point in the geometric model of the first-stage automatic leveling mechanism shown in Fig. 3 indicate that the support ball hinge and support platform will move during the leveling process. If

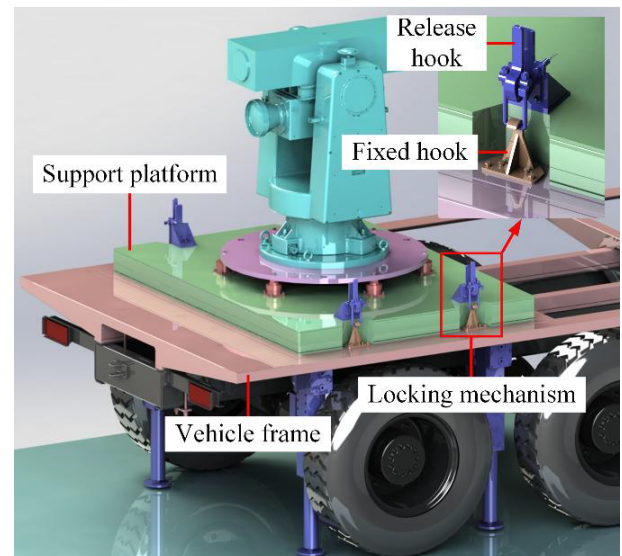


Fig. 4 Locking mechanism.

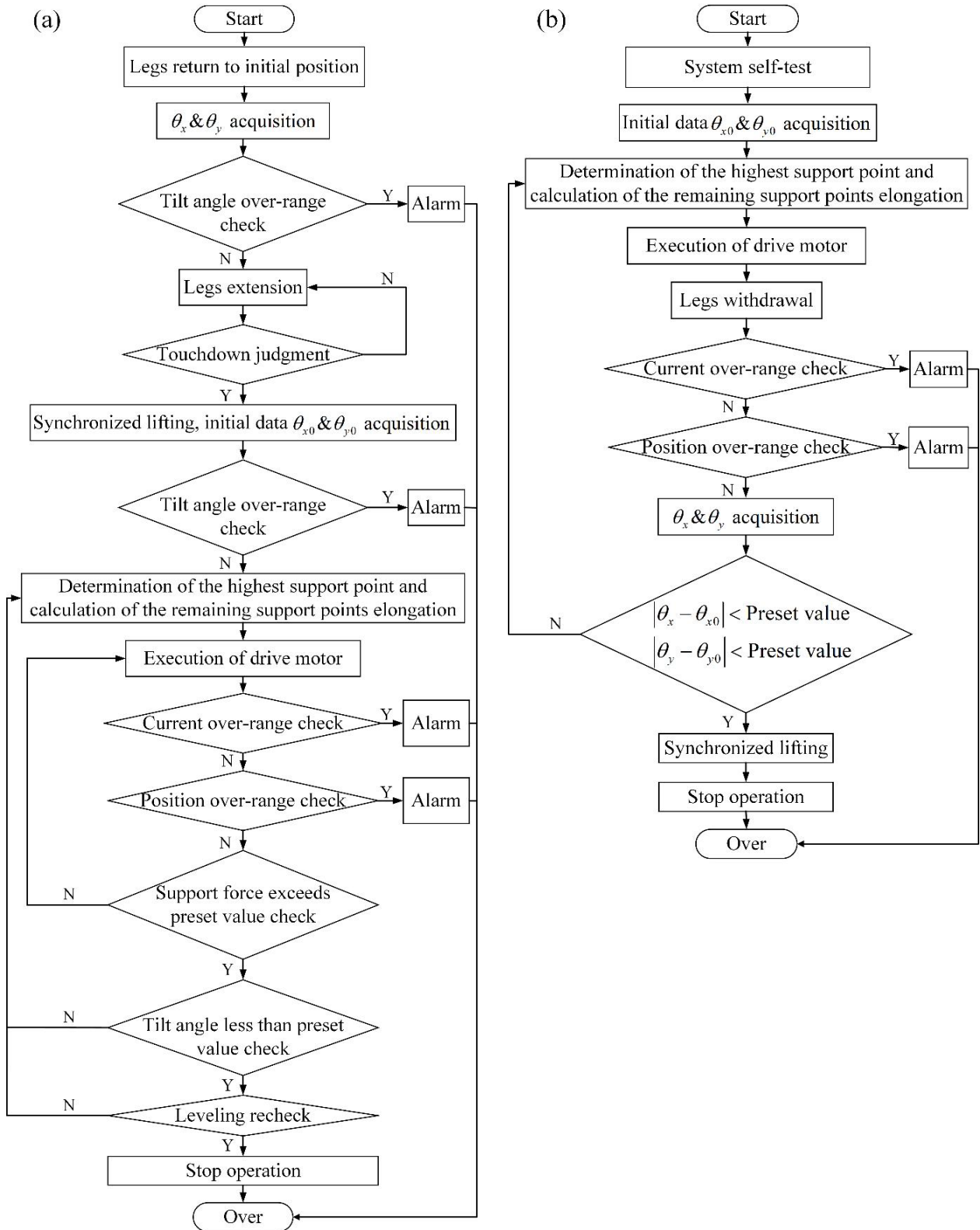


Fig. 5 Control flow chart of the first-stage automatic leveling mechanism. (a) Unfolding process, (b) withdrawal process.

the leveling legs are not controlled, it cannot ensure the accurate locking of the locking mechanism when the support platform is returned to the vehicle frame.

Based on the above analysis, the highest point chasing type angular error leveling control principle is used for the designed first-stage automatic leveling mechanism [29]–

[32]. The leveling control method based on repeated positioning is established to strictly limit the spatial movement path of each equivalent contact center point during the leveling unfolding and withdrawal process. This can ensure the accurate locking of the locking mechanism when the support platform falls back.

As shown in Fig. 5, the control flow chart of the first-stage automatic leveling mechanism is established, and the unfolding and withdrawal process can be divided into eight motion stages, which represent leg extension, leg touching the ground, synchronous lifting, leg leveling, leveling maintenance, support platform back to the initial tilt angle, synchronous withdrawal, and withdrawal completion.

#### 4. Second-Stage Automatic Leveling Mechanism Design

##### 4.1 Second-Stage Automatic Leveling Mechanism Model

As shown in Fig. 6, the two-stage automatic leveling mechanism consists of three sets of wedge-type electromechanical leveling assembly, tilt sensor and a leveling control module. Three sets of wedge-type electromechanical leveling assembly are installed on the vertical axis housing at the bottom of the theodolite in an even distribution. The single wedge-type electromechanical leveling assembly consists of drive motor, gear pair, worm wheel, worm, lead screw, slip wedge, lifting wedge, locking screw, and locking spring. The two-stage automatic leveling mechanism is a three-point support ball hinge structure, which does not have the problem of “false leg”. And the axial force on the three equivalent support center points is the same.

The wedge-type electromechanical leveling assembly uses the transmission structure of gear pair, worm gear pair, screw pair and wedge plane pair to convert the rotational motion of the drive motor into a small amount of movement in the vertical direction of the wedge. The tilt sensor is used to transmit the attitude information of the vertical axis tilt of the theodolite to the leveling control module real-time. The feedback signal from the tilt sensor drives the wedge-type electromechanical leveling assembly to achieve the second-stage precision leveling of the theodolite.

Figure 7 shows the layout of the second-stage automatic leveling mechanism, points A, B, and C represent the equivalent support center points for three sets of wedge-type electromechanical leveling assembly respectively. Assuming that the angular resolution of the drive motor is  $\theta_{q2}$ , the gear ratio of the reducer composed of gear pair and worm gear pair is  $i_{q2}$ , the pitch of screw pair composed of the screw and the slip wedge is  $P_{q2}$ , and the tilt angle of tilting surface for slip wedge and lifting wedge is  $\theta_{xk}$ , the leveling angular resolution of the second-stage automatic leveling mechanism along the AD direction in Fig. 7 can be obtained

$$\Delta\theta_{qx} = \arctan\left(\frac{\theta_{q2} \cdot P_{q2} \cdot \tan \theta_{xk}}{540 \cdot i_{q2} \cdot R_{xk}}\right) \quad (20)$$

The leveling angular resolution of the second-stage auto-

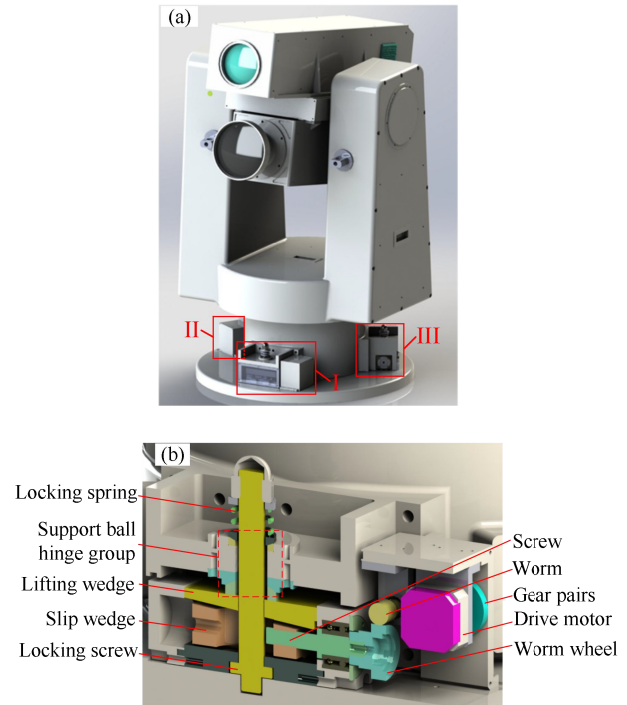


**Fig. 6** Physical model of the second-stage automatic leveling mechanism. (a) Installation layout of the wedge-type electromechanical leveling assembly, (b) wedge-type electromechanical leveling assembly.

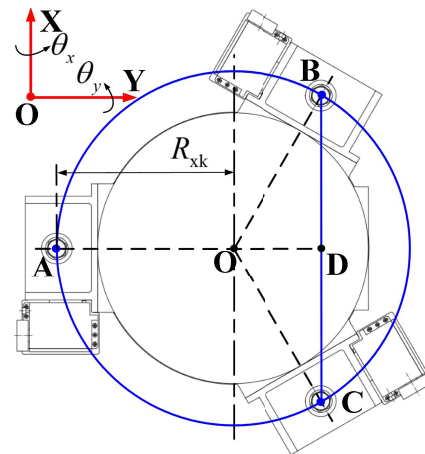


**Fig. 7** Layout of the second-stage leveling mechanism.

matic leveling mechanism along the BC direction in Fig. 7 can be obtained

$$\Delta\theta_{qy} = \arctan\left(\frac{\theta_{q2} \cdot P_{q2} \cdot \tan \theta_{xk}}{360 \sqrt{3} \cdot i_{q2} \cdot R_{xk}}\right) \quad (21)$$

To ensure that the wedge plane subsiding locking, and the second-stage automatic leveling mechanism has a large leveling range, the tilt angle of the tilting surface [14] satisfies

$$\theta_{xk} = 4^\circ \quad (22)$$

It can be seen from Eqs. (20), (21) and (22) that the second-stage automatic leveling mechanism has extremely high

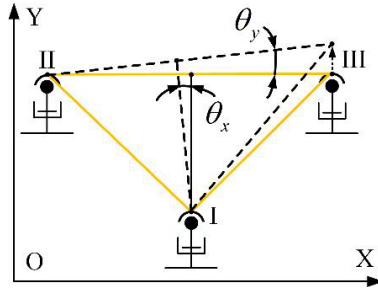


Fig. 8 Geometric model of the second-stage automatic leveling mechanism.

leveling resolution, which ensures the realizability of the second-stage precision automatic leveling for theodolites.

#### 4.2 Serial Leveling Control Method

As shown in Fig. 8, the second-stage automatic leveling mechanism is simplified to a three-point ball hinge support geometry model. When component II or III is moving, the vertical axis has tilts  $\theta_x$  and  $\theta_y$  around the X-axis and Y-axis respectively. At this time, there is motion coupling in the leveling of the second-stage automatic leveling mechanism. When component I is moving, the vertical axis only has the tilt amount  $\theta_x$  around the X-axis, but no tilt amount around the Y-axis. In this case, there is no motion coupling in the leveling of the second-stage automatic leveling mechanism. When components II and III are in the same direction of synchronous motion, the second leveling mechanism in the leveling also has no motion coupling. However, due to the errors in parts processing and assembly, the three sets of wedge-type electromechanical leveling assembly have different gear ratios from the theoretical gear ratio. Therefore, under the two working conditions of component I motion or component II and III synchronous motion, there will be weak coupling of structural motion in two directions in the leveling for the second-stage automatic leveling mechanism.

Based on the above analysis, for the designed second-stage automatic leveling mechanism, the highest point chasing type angular error leveling control principle is also used for serial cyclic leveling control. First, adjust the tilt amount  $\theta_y$ , and then adjust the tilt amount  $\theta_x$ . The required leveling accuracy of the theodolite is achieved after several cycles. The control flow chart of the second-stage automatic leveling mechanism is shown in Fig. 9.

### 5. “False Leg” Detection

#### 5.1 Leg Static Analysis

After each leg touches the ground, the automatic leveling mechanism not only needs to ensure that there is no “false leg” during the leveling process but also needs to ensure that the supporting force of each leg is close to or even the same after the leveling is completed. It can ensure that the theodolite has good support stability during the non-landing mea-

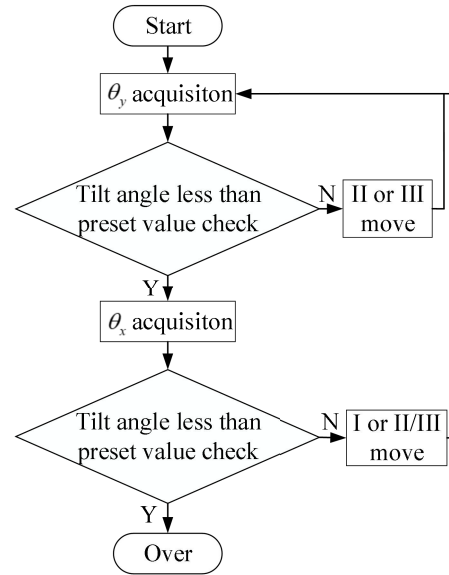


Fig. 9 Control flow chart of the second-stage automatic leveling mechanism.

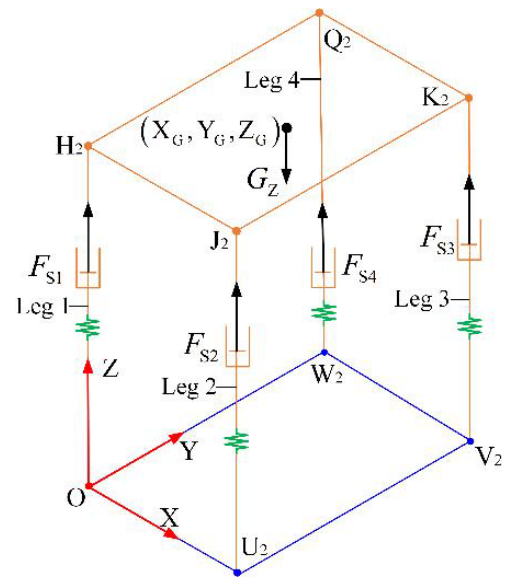


Fig. 10 Simplified mechanical model of the legs in leveling condition.

surement of the theodolite.

The simplified model of mechanics in leveling state is shown in Fig. 10, the support forces of the legs are  $F_{S1}$ ,  $F_{S2}$ ,  $F_{S3}$  and  $F_{S4}$ , and the total load of the legs is  $G_Z$ . The center of gravity of the total load is  $(X_G, Y_G)$  in the XOY plane. The support force of the leg is positive along the Z-axis, and the moment generated by the support force of the touchdown leg on the support platform satisfies Ampere’s rule.

The leg is in a state of balance, so there is a static equation as shown in Eq. (23).

$$\begin{cases} F_{S1} + F_{S2} + F_{S3} + F_{S4} - G_Z = 0 \\ (F_{S3} + F_{S4} - F_{S1} - F_{S2}) \cdot L_2 = G_Z L_2 - 2G_Z Y_G \\ (F_{S1} + F_{S4} - F_{S2} - F_{S3}) \cdot L_1 = 2G_Z X_G - G_Z L_1 \end{cases} \quad (23)$$

Then,

$$\begin{cases} F_{S2} = G_Z Y_G / L_2 - F_{S1} \\ F_{S3} = G_Z - G_Z X_G / L_1 - G_Z Y_G / L_2 + F_{S1} \\ F_{S4} = G_Z X_G / L_1 - F_{S1} \end{cases} \quad (24)$$

Considering the symmetrical design of the automatic leveling mechanism structure, the center of gravity of the total load can be approximated considered to be on the central axis of the leveling platform. Thus, there is  $X_G \approx \frac{L_1}{2}$  and  $Y_G \approx \frac{L_2}{2}$ , and Eq. (24) can be simplified as

$$\begin{cases} F_{S2} = G_Z / 2 - F_{S1} \\ F_{S3} = F_{S1} \\ F_{S4} = G_Z / 2 - F_{S1} \end{cases} \quad (25)$$

When  $F_{S1} = G_Z / 4$ ,  $F_{S1} = F_{S2} = F_{S3} = F_{S4} = G_Z / 4$  can be obtained from the Eq. (25).

Since the leg support is not rigid body support, the leg has elastic deformation in the balance state. Thus, when the automatic leveling mechanism is leveled to within the error range, a single leg micro-movement will occur when the leveling angle is still within the error range, but the support force of each leg still changes.

Suppose the support platform is in the horizontal state with  $\theta_x = 0$  and  $\theta_y = 0$ , the support force of the legs satisfies the Eq. (25). When the leg 1 has theoretical micro-elastic elongation  $\sigma_{Z1}$ , each leg will have micro-elastic deformation due to the change of the support force, which are  $\varepsilon_{Z1}$ ,  $\varepsilon_{Z2}$ ,  $\varepsilon_{Z3}$  and  $\varepsilon_{Z4}$  respectively. Compared with the legs, the support platform can be considered as a rigid model in the process of mechanical state change. After the micro-elastic deformation of each leg, the corresponding connection center points are still in the same plane, so that there is

$$\sigma_{Z1} - \varepsilon_{Z1} - \varepsilon_{Z3} = \varepsilon_{Z2} + \varepsilon_{Z4} \quad (26)$$

Assuming that the axial stiffness of leg support is  $K_{Z1}$ ,  $K_{Z2}$ ,  $K_{Z3}$  and  $K_{Z4}$  respectively, the total equivalent length of legs after extension, touching the ground, synchronous lifting and leveling is much larger than the difference of leg elongation caused by the initial value  $\theta_{x0}$  and  $\theta_{y0}$ . Therefore, it can be approximated as [33], [34]

$$K_Z \approx K_{Z1} \approx K_{Z2} \approx K_{Z3} \approx K_{Z4} \quad (27)$$

The change in the support force of each leg can be obtained

$$\begin{cases} \Delta F_{S1} = K_Z \cdot \varepsilon_{Z1} \\ \Delta F_{S2} = K_Z \cdot \varepsilon_{Z2} \\ \Delta F_{S3} = K_Z \cdot \varepsilon_{Z3} \\ \Delta F_{S4} = K_Z \cdot \varepsilon_{Z4} \end{cases} \quad (28)$$

The leg support force is

$$\begin{cases} F'_{S1} = F_{S1} + \Delta F_{S1} \\ F'_{S2} = F_{S2} - \Delta F_{S2} \\ F'_{S3} = F_{S3} + \Delta F_{S3} \\ F'_{S4} = F_{S4} - \Delta F_{S4} \end{cases} \quad (29)$$

At the same time, the support force of each leg still satisfies

$$\begin{cases} F'_{S1} + F'_{S2} + F'_{S3} + F'_{S4} - G_Z = 0 \\ F'_{S2} = G_Z / 2 - F'_{S1} \\ F'_{S3} = F'_{S1} \\ F'_{S4} = G_Z / 2 - F'_{S1} \end{cases} \quad (30)$$

thus

$$\varepsilon_{Z1} = \varepsilon_{Z2} = \varepsilon_{Z3} = \varepsilon_{Z4} = \sigma_{Z1} / 4 \quad (31)$$

Assume that the angular resolution of drive motor is  $\theta_{q1}$ , the reduction ratio of worm gear is  $i_{q1}$ , and the pitch of drive screw-nut pair is  $P_{q1}$ . The leveling line resolution of legs can be obtained

$$\Delta L_{q1} = \frac{\theta_{q1} \cdot P_{q1}}{360 \cdot i_{q1}} \quad (32)$$

When  $\sigma_{Z1} = \Delta L_{q1}$ , there is

$$\begin{cases} F'_{S1} = F_{S1} + \frac{K_Z \cdot \Delta L_{q1}}{4} \\ F'_{S2} = G_Z / 2 - F_{S1} - \frac{K_Z \cdot \Delta L_{q1}}{4} \\ F'_{S3} = F_{S1} + \frac{K_Z \cdot \Delta L_{q1}}{4} \\ F'_{S4} = G_Z / 2 - F_{S1} - \frac{K_Z \cdot \Delta L_{q1}}{4} \end{cases} \quad (33)$$

When  $\Delta L_{q1} = \frac{2G_Z - 4F_{S1}}{K_Z}$ , there is

$$\begin{cases} F'_{S1} = F'_{S3} = G_Z / 2 \\ F'_{S2} = F'_{S4} = 0 \end{cases} \quad (34)$$

From the Eq. (34), it can be seen that leg 2 and leg 4 become “false legs” with no support force while the mechanism is still in equilibrium. From the Eqs. (25) and (33), it can also be seen that the support force of the legs in the leveling state must be detected to ensure that the theodolite has good support stability during the non-landing measurement of theodolites.

## 5.2 “False Leg” Detection Method

As the automatic leveling mechanism itself has good rigidity, four points of support must have one more point of redundant support. In the process of leveling, the leg is under stress or not under stress, thus becoming a “false leg”.

Commonly used “false leg” detection methods include drive motor torque detection and support force detection

[9], [29]. When the drive motor torque detection method is used, the force on the leg touching the ground causes the drive motor torque to change. The drive motor torque increases with the increase of support force. The controller sets a certain threshold value of drive motor torque and detects the actual output torque of drive motor to determine the real and false legs. In line with the drive motor torque detection principle, the support force detection method uses force sensors to collect the support force of legs when the leg touches the ground. The controller sets the force threshold, and when the support force of legs is greater than the set force threshold, it is considered that the leg has touched the ground.

As shown in Fig. 11, the leg is modeled mechanically. Assuming that the output torque of drive motor is  $T_{q1}$  and the friction torque of worm support shaft is  $M_{G1}$ , the rotating torque of worm output is

$$T_{G1} = T_{q1} - M_{G1} \tag{35}$$

there is a rotating torque relationship between the worm wheel and the worm

$$T_{L1} = i_{q1} \cdot \eta_{G1} \cdot T_{G1} \tag{36}$$

where  $\eta_{G1}$  is the transmission efficiency of worm gear.

Assuming that the frictional torque of worm wheel support shaft is  $M_{L1}$  and the frictional torque of the screw support shaft is  $M_{S1}$ , then the output torque of screw is

$$T_{S1} = T_{L1} - M_{L1} - M_{S1} \tag{37}$$

For the Force Spiral Model, the relationship between the support force  $F_{S1}$  of the leg and the output torque  $T_{S1}$  of the screw is

$$T_{S1} = F_{S1} \cdot \frac{D_{S1}}{2} \cdot \tan(\psi_{S1} + \gamma_{S1}) \tag{38}$$

where  $D_{S1}$  is the middle diameter of the screw (unit: mm);  $\psi_{S1}$  is the lead angle of the screw (unit: °);  $\gamma_{S1}$  is the induced

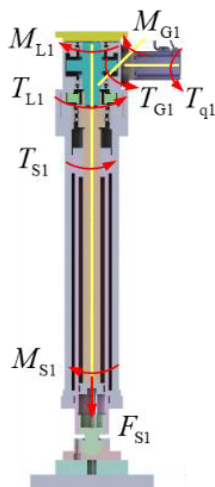


Fig. 11 Mechanical transfer model of the leg.

friction angle (unit: °).

From Eqs. (35), (36), (37) and (38), the relationship between the support force  $F_{S1}$  and the output torque  $T_{q1}$  can be expressed as

$$T_{q1} = \frac{F_{S1} \cdot \frac{D_{S1}}{2} \cdot \tan(\psi_{S1} + \gamma_{S1}) + M_{L1} + M_{S1}}{i_{q1} \cdot \eta_{G1}} + M_{G1} \tag{39}$$

Neglecting the friction torque of structural support shafts, Eq. (44) can be simplified as

$$T_{q1} = \frac{D_{S1} \cdot \tan(\psi_{S1} + \gamma_{S1})}{2 \cdot i_{q1} \cdot \eta_{G1}} F_{S1} = \kappa_1 \cdot F_{S1} \tag{40}$$

where  $\kappa_1$  is the conversion factor between the support force  $F_{S1}$  and the output torque  $T_{q1}$ , the value range is  $10^{-3} \sim 10^{-4}$ .

Therefore, “false leg” detection using the support force detection method is more sensitive compared with the method based on drive motor torque.

## 6. Performance Test of the Automatic Leveling Mechanism

As shown in Fig. 12, the automatic leveling mechanism was tested for unfolding and withdrawing. The initial accuracy calibration of tilt sensor was carried out with an electronic level, and the tilt angle sensor was used to collect data on the tilt angle  $\theta_x$  and  $\theta_y$  of the support platform. BWS2800-I dual-axis tilt sensor made by BWSENSING was selected

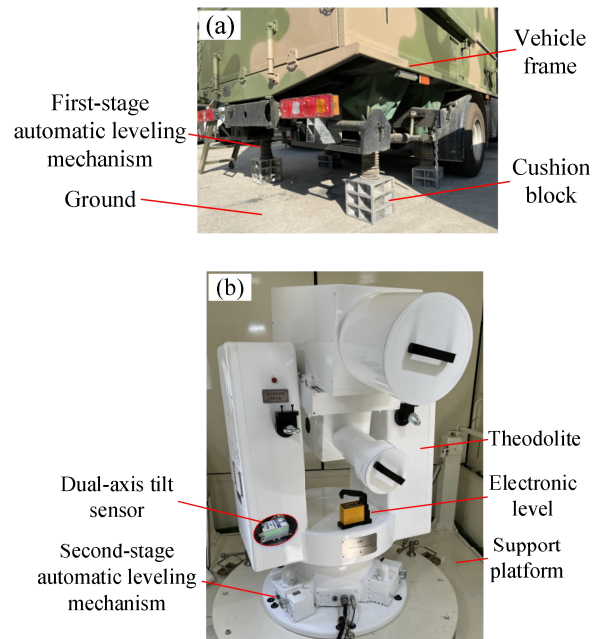


Fig. 12 Automatic leveling mechanism performance test. (a) External layout of the experimental platform, (b) internal layout of the experimental platform.

**Table 1** BWS2800-I dual-axis tilt sensor parameters.

Parameter	Measuring condition	Value
Measuring range (°)	Horizontal plane	±5
Measuring axis	Mutual vertical	X-Y
Accuracy (°)	Room temperature	0.001
Resolution (°)	Static	0.0005
Zero point temperature drift (°/°C)	-40~85°C	±0.0007
Cross-axis error (°)	-40~85°C	0.001
Output frequency (Hz)	5-100Hz	≤100

**Table 2** CAZF-LY88 spoke tension/pressure sensor parameters.

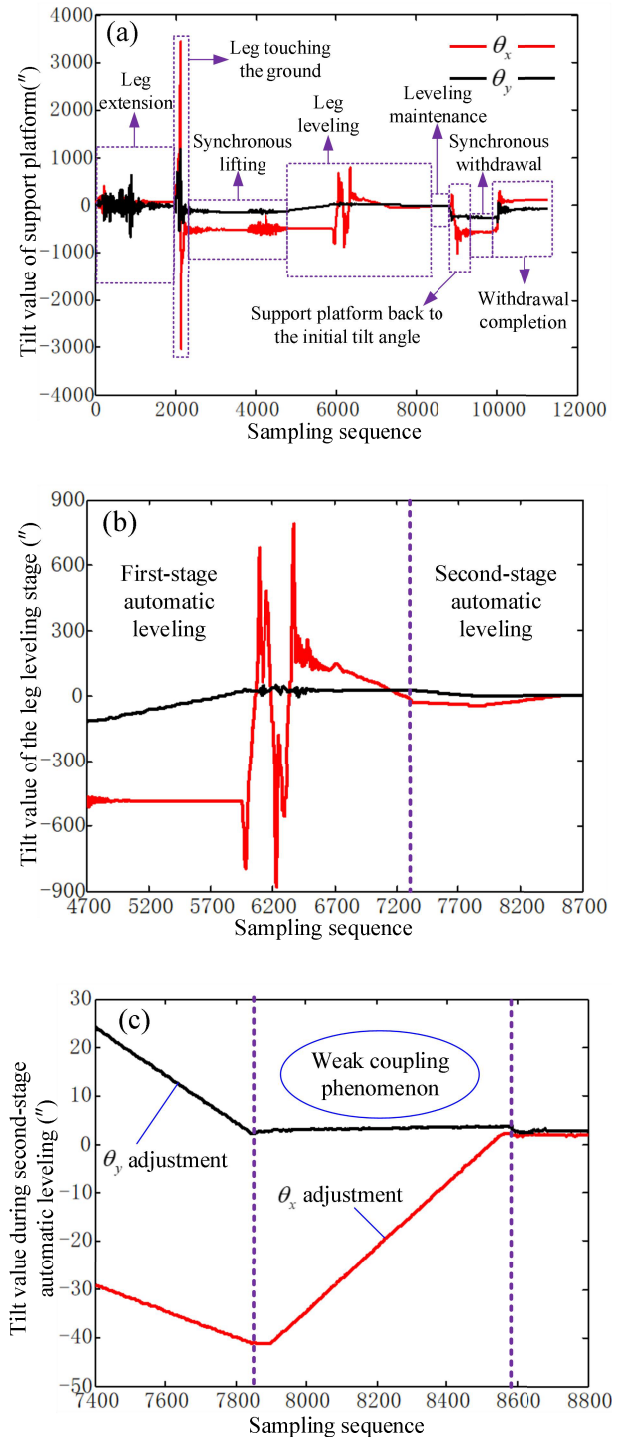
Parameter	Value
Capacity (kg)	2000
Total error (kg)	0.05%F.S
Non-linearity (kg)	0.05%F.S
Excitation voltage (V)	5-10
Operation temperature (°C)	-20~80

as the tilt sensor, and its parameters were shown in Table 1. Meanwhile, the support force detection method and the drive motor torque detection method were used to control the support force in the leveling process respectively. Besides, the force sensor was used to collect data on the support force of the leg. CAZF-LY88 spoke tension/pressure sensor made by CAZSENSOR was selected as the force sensor, and the parameters were shown in Table 2.

According to the tilt angle test data in Fig. 13(a), the eight stages of the unfolding and withdrawal process can be identified for the first-stage automatic leveling mechanism. At the same time, the support platform can be accurately retracted to the initial position in the five rounds of tests, which proved that the leveling control method based on repeated positioning can accurately control the space movement path of support platform and ensured the rapid withdrawal performance for high-mobility vehicle-mounted theodolites.

Figure 13(b) showed the tilt angle test data during the leg leveling stage. By leveling with the first-stage automatic leveling mechanism, the tilt angle  $\theta_x$  was reduced from  $-507.84''$  to  $-29.03''$ , and the tilt angle  $\theta_y$  was reduced from  $-116.04''$  to  $24.25''$ . Further, the tilt angle  $\theta_x$  was reduced to  $1.99''$ , and the tilt angle  $\theta_y$  was reduced to  $2.76''$  by leveling with the second-stage leveling mechanism. Since the accuracy of dual-axis tilt sensor used was  $3.6''$ , the vertical axis tilt angle can be adjusted to no more than  $3.6''$  by using the two-stage electromechanical automatic leveling mechanism. The total leveling time taken to complete from the leg extension stage to the leg leveling stage was 87 s since the data sampling frequency was 100 Hz during the test. It was worth noting that the total leveling time was not only related to the control strategy, but also to the initial tilt angles  $\theta_{x0}$  and  $\theta_{y0}$  of the support platform, as well as the speed of drive motor, the reduction ratio of transmission mechanism, and other factors.

It can be seen in Fig. 13(c),  $\theta_x$  changed significantly when the tilt angle  $\theta_y$  was adjusted. When the tilt angle  $\theta_x$  was adjusted,  $\theta_y$  exceeded the preset value due to the weak coupling effect of structure motion. Therefore, a second leveling cycle was required and the tilt angles  $\theta_x$  and  $\theta_y$  were

**Fig. 13** Tilt data of  $\theta_x$  and  $\theta_y$ . (a) Tilt data curve of unfolding and withdrawal process, (b) tilt data curve of the leg leveling stage, (c) tilt data curve of the second-stage automatic leveling.

finally adjusted to the current value range.

Figure 14 showed the support forces of the legs corresponding to eight stages during the unfolding and withdrawal of the theodolite. Between the leg leveling stage and the leveling maintenance stage, the leg micro-elongation

**Table 3** Support forces under support force detection method (N).

Test rounds	Leg 1	Leg 2	Leg 3	Leg 4	Total support force	Maximum deviation
1	7160.3	6400.3	7452.7	6651.5	27664.8	14.12%
2	6767.9	6863.6	6554.3	6921	27106.8	5.3%
3	7014.4	6662.3	6890.7	6432.6	27000	8.29%
4	7011.9	6737.7	6894.4	6558.8	27202.8	6.46%
5	7171.7	6559	7208.8	6573.8	27513.3	9.01%

**Table 4** Support forces under drive motor torque detection method (N).

Test rounds	Leg 1	Leg 2	Leg 3	Leg 4	Total support force	Maximum deviation
1	7964.4	4934.7	8672.8	5226.7	26798.6	43.1%
2	7363.4	6609.9	7102.9	5724.4	26800.6	22.26%
3	4517.7	8331.7	6793.3	6908.9	26551.6	45.78%
4	8991.4	8692.5	8373.5	1787.6	27845	80.12%
5	7978.8	7279.6	7136.4	4566.5	26961.3	42.77%

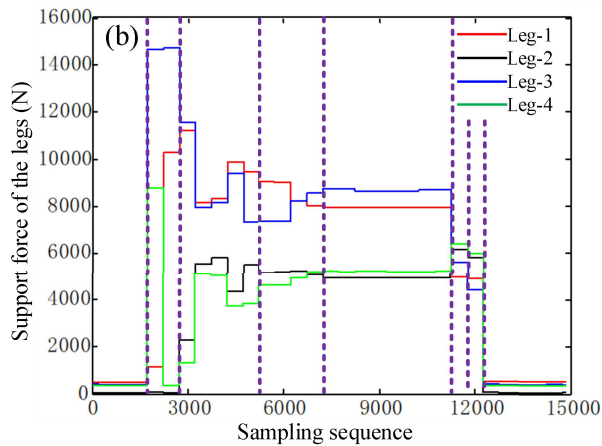
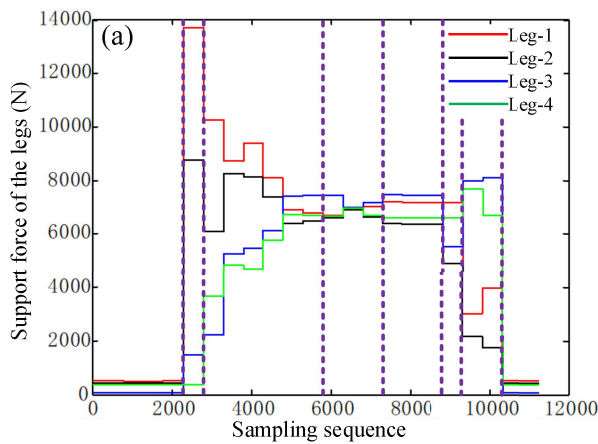


**Fig. 14** Support forces of the legs. (a) Support force data curve of support force detection method, (b) support force data curve of drive motor torque detection method.

caused a significant change in the support force, which proved the correctness of the mechanical characteristic analysis in Sect. 4.1.

The automatic leveling mechanism under the support force detection method and the drive motor torque detection method were leveled five times, and the support forces cor-

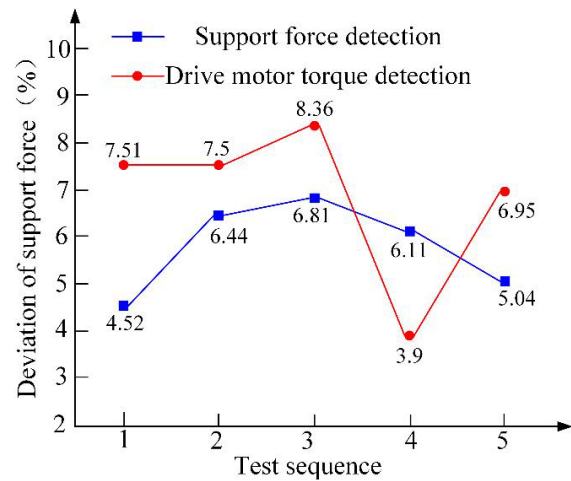


**Fig. 15** Deviation of support force under two detection methods.

responding to the leveling maintenance stage were obtained. The results were shown in Table 3 and Table 4. It can be seen that, based on the support force detection method, the support force of each leg in the leveling maintenance stage was guaranteed to be relatively average since the support force threshold was set in the leveling stage. The maximum support force error was 14.12%, and the average support force error was 8.64%. Besides, it had the characteristic that the support forces of diagonally opposite legs were close, which was consistent with the analysis of mechanical properties in Sect. 4.1.

However, based on the drive motor torque detection method, there was a large error in the support force of each leg in the leveling maintenance stage. The maximum support force error was 80.12%, and the leg support force was random. It was thus proved that the leveling mechanical properties based on support force detection method were significantly better than the drive motor torque detection method.

The mechanism used in the experiment was weighted, and the theoretical total load of the legs was  $G_Z = 28973.6\text{N}$ . Comparing the support force deviation under the two detection methods, the results were shown in Fig. 15.

Here, the maximum deviation of the leg pressure-based approach was only 8.36% (i.e., below 10%), which implies that the automatic leveling mechanism was mechanically stable with this method and that the force sensor was sufficiently sensitive for this application.

## 7. Conclusion

This paper studied the electromechanical automatic leveling mechanism for high-mobility vehicle-mounted theodolites. The innovation points of this paper are summarized as follows.

(1) A hierarchical automatic leveling strategy was proposed. The modeling and leveling control strategy of the first-stage automatic leveling mechanism and the second-stage automatic leveling mechanism were designed to realize the high-precision automatic leveling during the non-landing measurement of theodolites. Moreover, its leveling accuracy did not exceed 3.6" and the leveling time did not exceed 2 mins. It was worth noting that the leveling accuracy is limited by the accuracy of dual-axis tilt sensor, and the total leveling time is also the result of a specific condition.

(2) For the first-stage automatic leveling mechanism, a leveling control method based on repeated positioning was proposed to constrain the spatial movement path of each contact center point during the leveling process. Meanwhile, the eight motion stages of vehicle-mounted theodolites were accurately predicted to ensure the coincidence of spatial movement paths when the structural parts were unfolded and withdrawn. This provided important support to realize the rapid withdrawal for high-mobility vehicle-mounted theodolites. However, when the initial tilt angles of the support platform make the center point G of gravity of the total load beyond the legs, the leveling control method based on repeated positioning will not work. Therefore, the initial tilt angles of the support platform have a threshold range.

(3) The leg static balance equation and the mathematical model of "false leg" detection were established under the leveling state. The analysis results showed that the "false leg" detection using support force detection method was more sensitive compared with the method based on drive motor torque. Besides, experimental results verified that the maximum support force error based on the support force detection method was less than 15%, and the average error was less than 10%. In contrast, the maximum support force error based on the drive motor torque detection method reached 80.12%. Due to the structural complexity of the performance test, the center point G of gravity of the total load cannot be made consistent with the theoretical model, so the results of the support force have errors exist.

The hierarchical automatic leveling strategy and the two-stage electromechanical automatic leveling mechanism proposed in this paper can better meet the needs of vehicle-mounted theodolites for high-precision and fast leveling. They can also be used for vehicle-mounted radar, vehicle-mounted laser measurement devices, vehicle-mounted artillery launchers and other types of vehicle-mounted equip-

ment with high-precision and high-mobility working requirements. However, the issues of leveling accuracy and leveling efficiency based on this model still need to be further investigated.

## Acknowledgments

This work was supported by the National Natural Science Foundation of China (Grant No. 12103081).

## References

- [1] Z. He and B. Hu, *Photoelectric Measurement*, National Defense Industry Press, Beijing 2002 (in Chinese).
- [2] C.R. Smith, R. Grasso, J. Pledger, N. Murarka, D.H. Titterton, and M.A. Richardson, "Trends in electro-optical electronic warfare," *Technologies for Optical Countermeasures IX*, SPIE, vol.8543, 854302, 2012.
- [3] F. Prel, G.C. Holst, K.A. Krapels, L. Moreau, R. Bouchard, R.D. Bullis, C. Roy, C. Vallières, and L. Levesque, "Hyperspectral imaging spectro radiometer improves radiometric accuracy," *Infrared Imaging Systems: Design, Analysis, Modeling, and Testing XXIV*, SPIE, vol.8706, pp.249–260, 2013.
- [4] D. Ruffatto, H.D. Brown, R.H. Pohle, M.F. Reiley, D.D. Haddock, M.K. Masten, and L.A. Stockum, "Stabilized high-accuracy optical tracking system (SHOTS)," *Acquisition, Tracking, and Pointing XV*, SPIE, vol.4365, pp.10–18, 2001.
- [5] J.E. Harvey, A. Krywonos, and J.B. Houston, Jr., "Performance modeling of launch vehicle imaging telescopes," *Optical Modeling and Performance Predictions II*, SPIE, vol.5867, pp.125–136, 2005.
- [6] W. Tao, T. Jie, and S. Liwei, "Correction of the measuring error of vehicular photoelectric theodolite," *Infrared and Laser Engineering*, vol.41, no.5, pp.1335–1338, 2012 (in Chinese).
- [7] B. Zhang, "Research of photoelectric theodolite measurement method without landing," *Infrared*, vol.42, no.3, pp.36–42, 2021 (in Chinese).
- [8] X. Gang and S. Chai, "Optimal load balancing leveling method for multi-leg flexible platforms," *Chin. J. Mech. Eng.*, vol.26, no.5, pp.900–908, 2013.
- [9] H. Wu, S. Zhu, F. Zhang, X. Gang, C. Lyu, and A. Liu, "Design of automatic leveling control system for electromechanical support platform," *Journal of Shandong University of Technology (Natural Science Edition)*, vol.35, no.4, pp.29–35, 2021 (in Chinese).
- [10] W. Wang, X. Fu, Q. Lu, P. Xue, and X. Yue, "Design and implementation of automatic leveling control system for a rocket launcher ammunition supply vehicle," *Acta Armamentarii*, vol.43, no.S1, pp.82–87, 2022 (in Chinese).
- [11] X. Guo, W. Han, H. Chen, Q. Zhao, N. Zhang, F. Peng, S. Shou, "Strategy of automatic leveling control based on moving base," *Journal of Applied Optics*, vol.43, no.4, pp.618–625, 2022.
- [12] M. Zhang, "Design of auto leveling hydraulic system and analysis of fuzzy PID control," *Chinese Journal of Construction Machinery*, vol.19, no.05, pp.453–457+470, 2021.
- [13] Y. Pan, F. Zhao, J. Xiao, and R. Wu, "Simulation research on hydraulic leveling system of vehicle-mounted radar," *J. Phys.: Conf. Ser.*, vol.2355, no.1, 012064, 2022.
- [14] J.-F. Du, "Design of the wedge leveller," *Optics and Precision Engineering*, vol.11, no.03, pp.301–304, 2003.
- [15] C. Liu and Z. He, "Design of automatic leveling and centering system based on error correction and compensation algorithm," *5th International Symposium on Advanced Optical Manufacturing and Testing Technologies: Smart Structures and Materials in Manufacturing and Testing*, SPIE, vol.7659, pp.179–184, 2010.
- [16] C. Liu, Z. He, X. Huang, and Y. Zhan, "Design of automatic leveling and centering system of theodolite," *6th International Symposium on*

Advanced Optical Manufacturing and Testing Technologies: Large Mirrors and Telescopes, SPIE, vol.8415, pp.204–210, 2012.

- [17] Z. He, X. Huang, C. Liu, Y. Zhang, J. Du, “General design of automatic leveling and centering system of theodolite,” *Journal of Gun Launch & Control*, no.1, pp.42–46, 2013 (in Chinese).
- [18] Y. Cao, M. Wang, Y. Yu, T. Wang, D. Wang, G. Tong, and J. Sun, “Measurement and data processing of tilted platform for vehicular optical measurement equipment,” *Infrared and Laser Engineering*, vol.43, no.08, pp.2704–2708, 2014 (in Chinese).
- [19] B. Jiang, S. Zhou, K. Jiang, H. Fu, and C. Mei, “Analysis of vertical axis error of vehicular theodolite,” *Infrared and Laser Engineering*, vol.44, no.05, pp.1623–1627, 2015 (in Chinese).
- [20] J. Luo, P. Xu, N. Pan, P. Jiang, X. Li, and H. Zhang, “Non-landing vehicle-mounted electro-optical theodolite deformation measurement method using inertial sensors,” *Measurement Science and Technology*, vol.30, p.055103, 2019.
- [21] J. Luo, Y. Fan, P. Jiang, Z. He, P. Xu, X. Li, W. Yang, W. Zhou, and S. Ma, “Vehicle platform attitude estimation method based on adaptive Kalman filter and sliding window least squares,” *Measurement Science and Technology*, vol.32, no.3, 035007, 2020.
- [22] Q. Yu, G. Jiang, S. Fu, Z. Chao, Y. Shang, and X. Sun, “Fold-ray videometrics method for the deformation measurement of noninter-visible large structures,” *Appl. Opt.*, vol.48, no.24, pp.4683–4687, 2009.
- [23] J.B. Liu, X.H. Zhang, H.B. Liu, Y. Yuan, Z. Zhu, and Q. Yu, “Correction method for non-landing measuring of vehicle-mounted theodolite based on static datum conversion,” *Sci. China Technol. Sci.*, vol.56, pp.2268–2277, 2013.
- [24] J. Liu, X. Zhang, H. Liu, Y. Yuan, Z. Zhu, and Q. Yu, “New method for camera pose estimation based on line correspondence,” *Sci. China Technol. Sci.*, vol.56, pp.2787–2797, 2013.
- [25] H.B. Liu, C. Sun, Y.Q. Zhang, X. Liu, J. Liu, X. Zhang, and Q. Yu, “Hull deformation measurement for spacecraft TT&C ship by Photogrammetry,” *Sci. China Technol. Sci.*, vol.58, pp.1339–1347, 2015.
- [26] W. Jiang, Y. Gao, D. Feng, Z. Chen, and J. Pu, “Automatic-leveling system for base-plane of large-size photoelectric equipment,” *Optics and Precision Engineering*, vol.17, no.05, pp.1039–1045 2009 (in Chinese).
- [27] H. Wang, “A mechanical design of leveling jacks of vehicular radars,” *RADAR & ECM*, vol.35, no.2, pp.49–51, 2015 (in Chinese).
- [28] G. Wei, Y. Zhao, N. He, et al., “Design of electromechanical automatic leveling device based on ansys workbench,” *Ordnance Industry Automation*, vol.11, no.40, pp.11–15, 2021 (in Chinese).
- [29] H. Yang and G. Li, “Research on an automatically leveling control system for vehicle-borne platform with high accuracy,” *2006 2nd IEEE/ASME International Conference on Mechatronics and Embedded Systems and Applications*, IEEE, pp.1–5, 2006.
- [30] H. Yang and G. Li, “Study on leveling method and control technology of a vehicle-borne platform,” *Machinery Design & Manufacture*, no.12, pp.134–136, 2008 (in Chinese).
- [31] L. Guo, H. Tan, and M. Zeng, “Design of automatic leveling control system for special vehicle-mounted platform,” *2022 International Conference on Artificial Intelligence and Computer Information Technology (AICIT)*, IEEE, pp.1–5, 2022.
- [32] W. Su, B. Deng, B. Song, and Q. Guo, “The fast leveling strategy and intelligent control of automatic vehicle leveling device,” *Mechanical Science and Technology for Aerospace Engineering*, vol.33, no.12, pp.1897–1901, 2014 (in Chinese).
- [33] M.H. Jones and S.A. Velinsky, “Stiffness of the roller screw mechanism by the direct method,” *Mechanics Based Design of Structures and Machines*, vol.42, no.1, pp.17–34, 2014.
- [34] F. Zhai, Y. Yin, C. Li, W. Tian, and Z. Qiao, “Stiffness modeling and feedforward control of servo electric cylinder drive system,” *Journal of Jilin University (Engineering and Technology Edition)*, vol.51, no.2, pp.442–449, 2021 (in Chinese).



**Xiangyu Li** is a doctoral candidate, Master, Graduated from Xi’an Jiaotong University in 2016. Worked in Xi’an Institute of Optics and Precision Mechanics, Chinese Academy of Sciences. His research interests include optical precision instrument design.



**Ping Ruan** is a professor, Doctor, graduated from University of Chinese Academy of Sciences in 2003. Worked in Xi’an Institute of Optics and Precision Mechanics, Chinese Academy of Science. Her research interests include overall design of the optical remote sensing instruments and the optical precision instruments.



**Wei Hao** is a professor, Doctor, graduated from University of Chinese Academy of Sciences in 2007. Worked in Xi’an Institute of Optics and Precision Mechanics, Chinese Academy of Science. His research interests include photoelectric detection and imaging methods.



**Meilin Xie** is an associate professor, Doctor, graduated from University of Chinese Academy of Sciences in 2020. Worked in Xi’an Institute of Optics and Precision Mechanics, Chinese Academy of Sciences. His research interests include photoelectric detection and imaging methods.



**Tao Lv** is an associate professor, Master, graduated from Xi’an Jiaotong University in 2014. Worked in Xi’an Institute of Optics and Precision Mechanics, Chinese Academy of Sciences. His research interests include optical precision instrument design.